ELSEVIER

Journal of Nuclear Materials 244 (1997) 36–43

journal of nuclear materials

Measurement of 2000–2100°C oxygen diffusion coefficients in hypostoichiometric UO_2

P.J. Hayward [a], I.M. George [a], R.A Kaatz [b], D.R. Olander [c,*]

[a] *Containment Analysis, AECL Research, Whiteshell Laboratories, Pinawa, MB, Canada R0E 1L0*
[b] *Analytical Science Branches, AECL Research, Whiteshell Laboratories, Pinawa, MB, Canada R0E 1L0*
[c] *Department of Nuclear Engineering, University of California, Berkeley, CA 94720, USA*

Received 16 July 1996; accepted 12 November 1996

Abstract

The chemical diffusion coefficient of oxygen in UO_{2-x} has been measured using molten Zircaloy held in a UO_2 crucible to establish the concentration driving force. The oxygen-to-uranium distribution set up by this method was determined by scanning electron microscopy/image analysis of the number density and area fraction of uranium metal precipitates that form when UO_{2-x} disproportionates upon cooling. Oxygen diffusivities were determined by fitting the numerical solution of Fick's second law to the O/U profiles. The diffusion coefficients are $(3.3 \pm 0.5) \times 10^{-8}$ m^2/s at 2000°C and $(3.6 \pm 0.8) \times 10^{-8}$ m^2/s at 2100°C.

1. Introduction

Several factors contribute to the inability to resolve the long-standing dispute over the theoretical interpretation of experiments on the dissolution of UO_2 by molten Zircaloy [1–3]. The first is the difficulty of describing mass transport in a three-component system that contains two or more phases. The second is the paucity of equilibrium data at the temperatures of the experiments. Most analyses rely on an early measurement of the liquidus on the U–Zr–O ternary section at 2000°C. Third, transport properties of the system, particularly diffusion coefficients, are poorly-known. In particular, the chemical diffusion coefficient of oxygen in UO_{2-x} (D_0) affects the rate at which oxygen is added to the liquid from the solid oxide, and thereby affects fuel solubility in the melt.

A lower-bound estimate of D_0 at 2000°C of 3×10^{-8} m^2/s was provided by Kim and Olander [4]. This estimate was based on the absence of an O/U gradient in the walls of the crucibles used in the dissolution tests. Bayoglu and Lorenzelli's measurements of the oxygen chemical diffusivity in the mixed oxide (U, Pu)O_{2-x} up to 1400°C [5] give $D_0 = 1.4 \times 10^{-8}$ m^2/s when extrapolated to 2000°C. From Matzke's [6] review, D_0 in UO_{2+x} lies in the range 1×10^{-8} to 8×10 m^2/s at 2000°C. However, owing to the very different atomic mechanisms of oxygen migration in hypo-and hyperstoichiometric urania (i.e., vacancy versus interstitial mechanisms), estimates of D_0 in UO_{2+x} cannot be safely applied to UO_{2-x}.

The only experimental measurement of oxygen mobility in UO_{2-x} is the tracer-diffusivity experiment of Kim and Olander [7]. These have been converted to chemical diffusivities using the Darken relationship [8], leading to $D_0 \sim 3 \times 10^9$ m^2/s at 2000°C. This value is significantly lower than the estimates cited previously. Given the importance of D_0 in the modeling of UO_2 dissolution in molten Zircaloy(Zry), an experiment intended solely to determine this property was designed and executed.

The method used to measure D_0 was suggested by the previously-observed formation of U-metal precipitates within UO_2 after cooling of crucible-based test specimens used to study fuel dissolution in molten Zry [4,9]. The origin of these precipitates can be explained as follows. In addition to fuel dissolution that occurs when UO_2 is contacted by molten Zry, oxygen from the remaining solid diffuses into the melt, causing local reduction of UO_2 to

* Corresponding author.

PII S0022-3115(96)00722-2

UO_{2-x}. This process creates a gradient in the hypostoichiometry parameter, x, across the undissolved UO_{2-x} fuel. During subsequent cooling, disproportionation of the single-phase UO_{2-x} occurs according to

$$UO_2 \rightarrow \left(\frac{2-x}{2}\right)UO_2 + \frac{x}{2}U \quad (1)$$

giving stoichiometric UO_2 and exsolved U metal that appears as a precipitate phase. Thus, if the UO_2 has been heated isothermally in contact with molten Zry for a known time, the concentration gradient of U-metal precipitates across the cooled sample can be used to derive D_0 for hypostoichiometric urania.

2. Experimental

The oxide diffusion specimens were 20.5 mm tall, 14.2 mm O.D., 6.1 mm I.D. cylinders of UO_2 that had been fabricated from 97% dense fuel pellets. Before use, the top and bottom faces of each cylinder were ground and polished to a 6 μm finish. Cylindrical Zry4 pieces were machined from Teledyne Wall Chang bar stock to fit inside the UO_2 cylinders. The height of each metal insert was 10% less than that of the UO_2 cylinders to allow for expansion upon melting of the metal. The function of the Zry was, when melted, to reduce the O/U ratio of the oxide cylinder to the lower phase boundary of urania. This produces the oxygen concentration driving force that causes diffusional transport and sets up the O/U gradient that is measured at the end of the test.

Each experiment was performed inside a 16 mm I.D., 17.5 mm O.D., 22.5 mm tall thoria crucible to contain any melt leakage. The assembly configuration is shown in Fig. 1. A UO_2 cylinder containing a Zry charge was placed on a 14.2 mm diameter, 2 mm thick disk of high density yttria inside the thoria crucible. Yttria was chosen as the baseplate material because of its inertness in contact with molten Zry. Tile mating yttria and UO_2 bottom-wall surfaces had also been previously polished to 6 μm finishes to prevent molten metal leakage during the experiment.

Another UO_2 cylinder was placed on top of the first cylinder to perform the following functions: (i) to create an

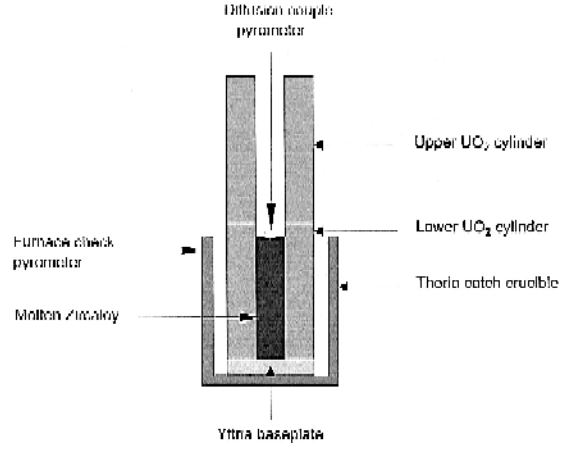

Fig. 1. Schematic diagram of UO_2/molten Zry diffusion couple assembly.

effective black body cavity for pyrometer measurement of the Zry temperature during the experiment; (ii) to shield the Zry charge from direct exposure to the furnace element; (iii) to prevent any melt from flowing over the top of the first cylinder; and (iv) to increase the load on the yttria baseplate, thereby minimizing any melt seepage. Finally, tile entire assembly was positioned in the hot zone of a Centorr tungsten resistance furnace coupled to a programmable controller via a type C thermocouple.

After evacuating and backfilling with ultra-high-purity argon, the furnace was ramped to 1000°C over 1 h. At this time, a previously-calibrated dual-wavelength pyrometer was focused on the top of the Zry charge through a quartz glass window in the furnace roof. The temperature recorded by this pyrometer was assumed to be the same as the UO_2 temperature. A similar pyrometer, focused on the lip of the thoria crucible through a quartz glass window in the furnace sidewall, was used to check the furnace temperature. The outputs from both pyrometers were fed into a computer-based data acquisition system and recorded at 1 s intervals.

After the hold at 1000°C, the assembly was heated to 1500°C over 5 min and then ramped to the test temperature

Table 1
Experimental parameters

Experiment no.	Target time (s) and temperature (°C)	Total time molten (s)	Main part of isotherm
5	180, 2000	190	2000 – 16°C for 150 s
6	180, 2000	192	1998 – 12°C for 159 s
7	120, 2000	152	2003 – 17°C for 106 s
8	120, 2000	138	2007 – 13°C for 92 s
10	300, 2000	336	2003 – 10°C for 277 s
11	300, 2000	321	2006 – 10°C for 277 s
12	100, 2100	123	2089 – 29°C for 77 s
15	150, 2100	187	2100 – 14°C for 121 s
16	200, 2100	276	2100 – 16°C for 216 s

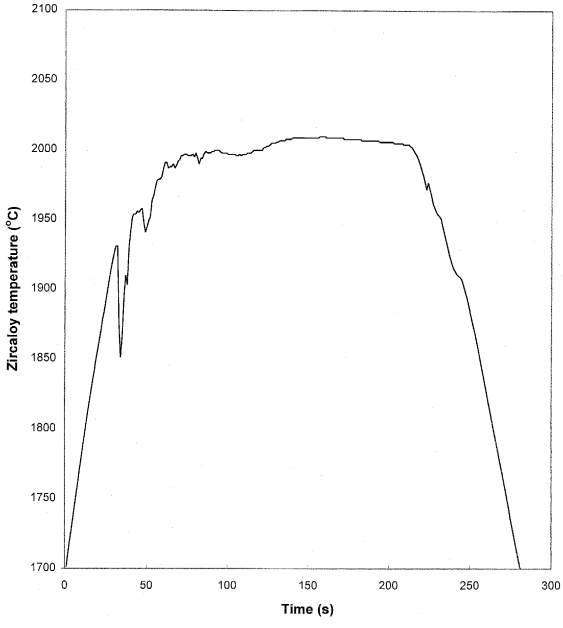

Fig. 2. Time/temperature trace for Test 6 specimen.

(2000 or 2100°C) at the maximum rate achievable. Typically, this rate was ~9°C/s over most of the ramp range, falling as the set point was approached. The specimen was held at the target temperature for the desired time (300 s at 2000°C or 200 s at 2100°C) and then cooled rapidly (5°C/s) to 1500°C, followed by cooling to room temperature over 1 h.

The parameter for the nine experiments performed are summarized in Table 1. Fig. 2 shows a representative time/temperature trace for the Test 6 sample. Because O diffusion occurs at all temperatures where UO_2 is in contact with the melt, the time intervals between Zry melting and attainment of the isotherm and between the start of cooling and melt freezing are important. The times at which melting and freezing occurred were clearly visible as discontinuities (caused by thermal arrests and/or emissivity changes) in the heating and cooling sections, respectively, in each time/temperature trace (see Fig. 2). Hence, the 'Total time molten' listed in Table 1 refers to the elapsed time between melting and freezing, while the 'Main part of isotherm' is included to indicate the degree of temperature control achieved during the 'soak' period.

3. Scanning electron microscopy and image analysis

After retrieval from the furnace and removal of the upper UO_2 cylinder and yttria baseplate, each UO_2/Zry diffusion couple was sectioned along the longitudinal mid-plane with a diamond wafer saw. The sections were ground and polished to 1 μm finishes and then carbon coated in preparation for scanning electron microscope (SEM) examination, using a JEOL JSM-6300V instrument. Image analyses were performed with Link-Isis-IMquant software on backscattered electron micrographs to make use of the atomic number contrast between the various phases present in each sample.

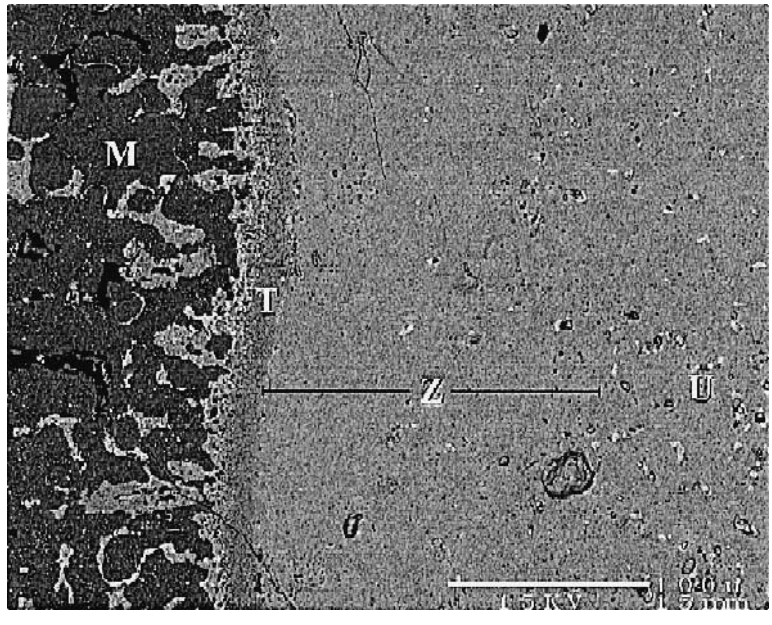

Fig. 3. Backscattered electron micrograph of the melt/crucible interface from test 6 showing: two-phase melt (M); transition zone (F); U-free zone (Z); and U-metal precipitates + associated voids in the remaining UO_2 regions (U).

Fig. 3 illustrates a typical melt/UO_2 interface at the midpoint of the right-hand cylinder wall in the Test 6 specimen. The micrograph shows similar features to those described previously in specimens from UO_2/molten Zry dissolution tests at 2000–2100°C [4,9]. The melt region consists of a two-phase assemblage of (U, Zi)O_{2-x} and α-Zr(O). A thin 'transition zone' occurs at the melt/cylinder interface. Adjacent to the transition zone is a ~150 μm wide zone in which the U-metal precipitates and their associated pores are almost completely absent (the 'U-free zone'). The remaining regions in the sample contain the U-metal precipitates, which had formed generally at UO_2 grain boundaries. The precipitates seen as white spots in Fig. 3, show good tone contrast with the UO_2 matrix (gray) and voids (black), making them ideal for measurement of the U-metal distribution by image analysis.

The image analyses were performed as follows. With the SEM magnification set at ×300, separate traverses were made across the left-hand and right-hand cylinder walls of the oxide crucible at approximately mid-height. Each traverse started at the point where U precipitates began to occur in the UO_2-matrix and finished at the outer edge of the cylinder wall. Care was taken to ensure that there was no overlap in the fields of view during this process. For each field of view, the SEM magnification was increased to ×600 and a digital micrograph was recorded. The higher magnification was used to give better resolution of the U precipitates in terms of image pixels, even though this meant that only the central 25% of each ×300 field of view was sampled. Finally, the volume percent U and the number of U precipitates in each micrograph as were determined as functions of the distance between the melt centerline and the mid-point of each ×600 image.

The image analyzer provides data on the areal number density of precipitate particles and the area fraction of the intersected spheres on the plane of the section. These are converted to the stoichiometry-deviation parameter x in UO_{2-x} as shown in Appendix A. Thus the information available for determination of D_0 consists of the stoichiometry profile $x(r)$ at a known time t of contact between the molten Zry and the oxide crucible.

4. Calculation of oxygen diffusion coefficients

Most studies dealing with the chemical diffusivity of oxygen in $UO_{2\pm x}$ have found the diffusivity to be independent of x [8,10]. However, from oxidation/reduction experiments on (U, Pu)$O_{2\pm x}$ at temperatures <1000°C, Bayoglu and Lorenzelli [11] have demonstrated a distinct x-dependence close to exact stoichiometry. In their 'recalculated' results, the oxygen diffusion coefficient D_0 decreases by a factor of ~2 in the range $0 < x < 0.01$, but is nearly constant for larger x. Since the range of stoichiometry deviation in the specimens tested in the present study is from $x = 0$ to $x = 0.20$, the increase in D_0 very close to exact stoichiometry should not significantly affect data interpretation. With the assumption of a composition-independent oxygen diffusivity and a predominantly radial oxygen flux, the system was analyzed using the one-dimensional cylindrical diffusion equation:

$$\frac{\partial x}{\partial t} = \frac{D_0}{r}\frac{\partial}{\partial r}\left(r\frac{\partial x}{\partial r}\right). \quad (2)$$

The initial condition corresponds to stoichiometric UO_2:

$$x = 0 \quad \text{at } t = 0. \quad (3)$$

The boundary conditions are

$$x = x_0 \quad \text{at } r = a, \quad (4)$$

$$(\partial x/\partial r) = 0 \quad \text{at } r = b, \quad (5)$$

where a and b are the inner and outer radii of the UO_2 crucible, respectively. The ratio of b to a in the present design is 2.36.

Eq. (5) represents the no-flux condition at the crucible outer surface. Eq. (4) assumes that the stoichiometry of the oxide at the inner surface is that of the lower phase boundary of pure urania at the temperature of the anneal.

The complications of the moving boundary at $r = a$ have been ignored in the analysis. The significance of the moving-boundary effect was approximately assessed by solving the diffusion equation in a semi-infinite slab with the spatial coordinate z fixed on the moving boundary. This motion induces a convective term $v\partial x/\partial z$ into Fick's second law, where v is the boundary velocity. The analytical solution to this problem is possible if $v = k/t^{1/2}$ (see Eqs. (42)–(46) of Ref. [12]). For the present application, the parameter k was estimated from the measured change in the thickness of the crucible wall during the diffusion anneals and the formula: $\Delta(\text{thickness}) = 2kt^{1/2}$. At 2000°C, wall thinning is ~5% of the initial thickness while at 2100°C, it is ~13%. For typical anneal times, the error in the concentration distribution incurred by ignoring the moving boundary effect is ~5%, which is well within the accuracy of the measurements.

The precipitate-free zone at the inner surface of the crucible was ignored in the fitting. The absence of U metal precipitates in this zone does not mean that the oxide was not reduced here. Rather, it means that the presence of zirconium stabilizes the defect structure of the oxide so that it does not convert to a stoichiometric oxide upon cooling. In addition, the data points nearest this zone were generally aberrant and were ignored. Similarly, the outermost points (near $r = b$) often were too low because the SEM window fell off the edge of the sample, and these points were also ignored in data fitting. Points which were obviously far away from the general trend of the remainder of the data were also neglected.

Fitting was done by selecting values of D_0 and x_0 that best fit the data. Because of the way that these parameters

enter the theory, fitting was sequential. The diffusivity D_0 controls the shape of the profile (i.e., small D_0 gives a steep gradient; large D_0 tends to give a flat profile). The lower-phase-boundary oxygen concentration represented by x_0 controls the scale of the distribution. Thus, fitting proceeded as follows: For each experiment, a value of D_0

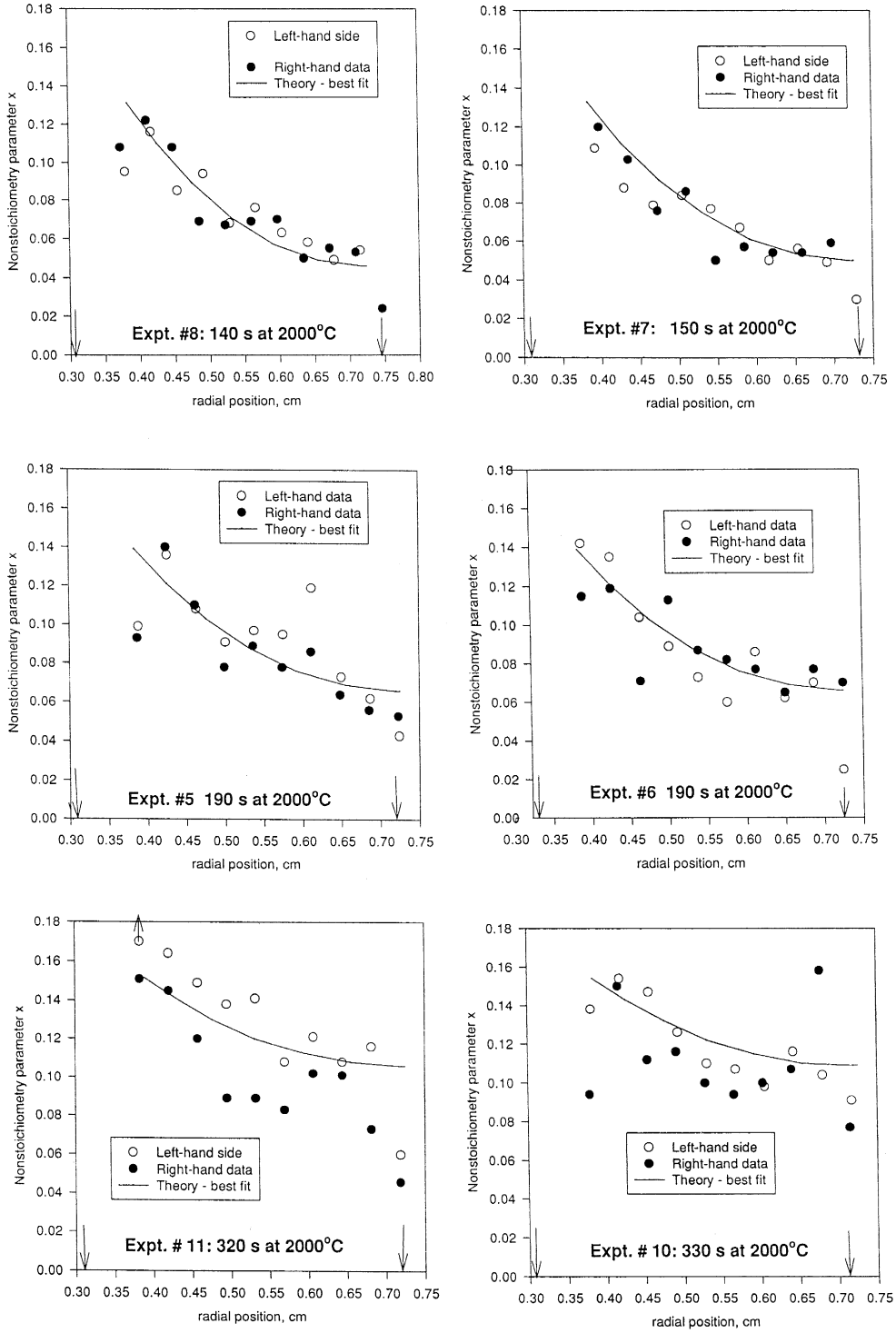

Fig. 4. Fitting of diffusion theory (curve) to the data at 2000°C.

Table 2
Fitting the theory to experiment at 2000°C

Expt. no.	Time (s)	$D_0 \times 10^8$ (m^2/s)	x_0	Error
5	190	3.0	0.20	0.09
6	190	3.5	0.18	0.09
7	150	4.0	0.18	0.09
8	140	4.0	0.17	0.08
10	330	2.5	0.20	0.08
11	320	3.0	0.19	0.13

was assumed, the diffusion equation was solved numerically, and then the value of x_0 that gave the smallest deviation between the theoretical values and the data was determined. (Both the ''left-side'' and ''right-side'' data were used in fitting.) This procedure was repeated for a number of values of D_0 and the deviation from the data noted. The value of D_0 (and its associated x_0 value) that gave the smallest error measure was taken as the best fit for this experiment. Table 2 shows the best fits for the six experiments at 2000°C.

There is remarkably good consistency between all six experiments at this temperature with regard to the best-fitting values of the diffusion coefficient and the lower phase boundary composition. At 2000°C, these are

$$D = (3.3. \pm 0.5) \times 10^{-8}\ \mathrm{m^2/s} \text{ and } x_0 = 0.18 \pm 0.02.$$

The lower phase boundary estimated from the data is within the range of accepted values [13].

At 2100°C, the data from run No. 12 could not be fitted to the theory, even discarding obviously errant points. The fact that the temperature continually increased during this experiment may have contributed, but the shape of the oxygen deficit distribution is opposite what one would have expected from the imposed temperature transient. The remaining two experiments at this temperature were not as easily fit as those at 2000°C. The contact times used in the numerical analysis were not those given in Table 1 for these experiments. Rather, they were simply approximated from the time-temperature traces. A range of D_0 and x_0 values produced approximately the same error, so distinct values of these parameters were harder to select than was the case at 2000°C. Table 3 shows the results for 2100°C.

The agreement of the fits for the two anneal times is satisfactory, and gives the following (approximate) diffusivities and lower phase boundary concentrations at 2100°C:

$$D = (3.6 \pm 0.8) \times 10^{-8}\ \mathrm{m^2/s} \text{ and } x_0 = 0.29 \pm 0.03.$$

Table 3
Fitting the theory to experiment at 2100°C

Expt. no.	Time (s)	$D_0 \times 10^8$ (m^2/s)	x_0	Error
15	150	3–4	0.29–0.36	0.10
16	230	4–6	0.21–0.27	0.06

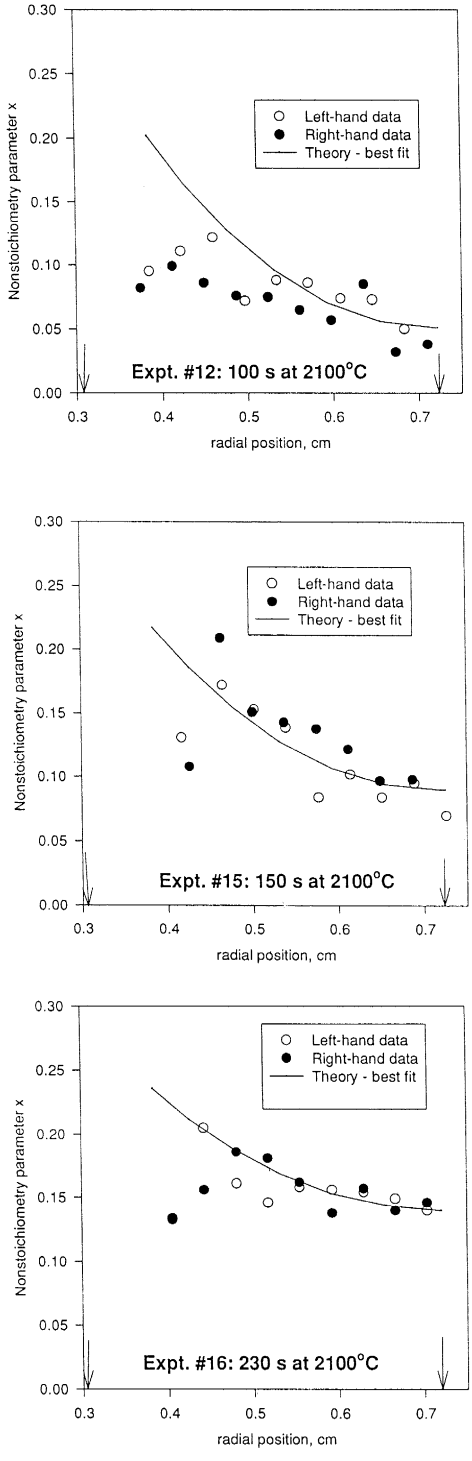

Fig. 5. Fitting of diffusion theory (curve) to the data at 2100°C. The data for Test 12 were not used in the fitting procedure.

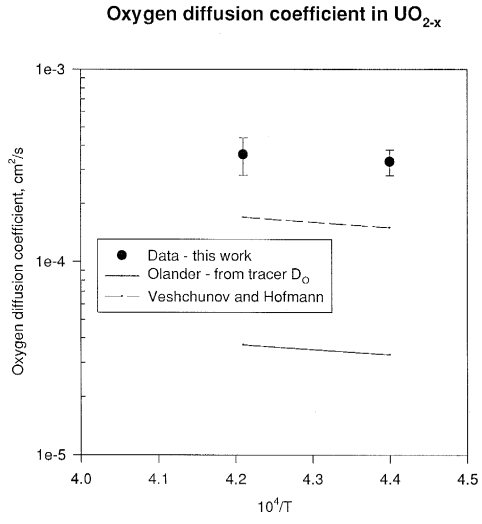

Fig. 6. Comparison of experimental oxygen diffusivities with prior estimates (Refs. [1,8]). The line for Ref. [8] represents an extrapolation from the temperature range 1200–1550°C.

Figs. 4 and 5 show the theoretical curves drawn through the data using the parameters given above for the two temperatures. The fits at 2000°C are quite satisfactory, with perhaps a slight net overestimate of the data in Experiment No. 10. The upper in Fig. 5 shows the data for Experiment No. 12 and the theoretical curve based on the parameters determined from the fitting of Experiments No. 15 and 16. For this curve, the equivalent time at 2100°C was taken to be 85 s

Fig. 6 compares the experimental results with the predictions of Olander [8] and Veshchunov and Hofmann [1]. The present data are greater than both, but closer to the latter than to the former.

Appendix A. Conversion of image-analyzer data to oxygen deficiency

Determination of the oxygen diffusivity in UO_{2-x} requires that the O/U ratio, or the stoichiometry deficit x, be known as a function of radial position. First, x is expressed in terms of the volume fraction v of metallic uranium in the cooled specimens produced by Eq. (1) of the text.

Starting with one mole of UO_{2-x}, the volumes of UO_2 and U produced by the disproportionation reaction are

$$V_{ox} = \left(1 - \frac{x}{2}\right) \div 0.041 \frac{\text{moles } UO_2}{\text{cm}^3} = 24.4\left(1 - \frac{x}{2}\right) \text{cm}^3,$$

$$V_U = \frac{x}{2} \div 0.080 \frac{\text{moles U}}{\text{cm}^3} = 6.25x \text{ cm}^3.$$

Because x is small compared to unity, the volume fraction of metal is approximately the ratio of V_U to V_{ox}, or

$$v = \frac{6.25}{24.4} x \text{ or } x = 3.9v. \quad \text{(A.1)}$$

The next step is to convert the metal area fraction and areal density data produced by the image analyzer to the volume fraction for use in Eq. (A.1). When cut by a plane, a random array of N spheres per unit volume each of radius R produces circles that are on average spaced apart by a distance [14]

$$L = \frac{1}{\sqrt{2RN}}.$$

Instead of the separation distance L, the areal number density on the plane n is directly measured by the image analyzer:

$$n = \frac{1}{L_2} = 2RN. \quad \text{(A.2)}$$

The plane does not cut all of the spheres at the equator, but the average radius of the circular intersections can be shown to be

$$r = \frac{\pi}{4} R. \quad \text{(A.3)}$$

The area fraction of the intersected spheres on the plane (which is measured by the image analyzer) is

$$a = \pi r^2 n. \quad \text{(A.4)}$$

Substituting Eqs. (A.2) and (A.3) into Eq. (A.4) yields

$$a = \frac{\pi^3}{8} R^3 N. \quad \text{(A.5)}$$

The volume fraction of metallic uranium is

$$v = \frac{4}{3} \pi R^3 N. \quad \text{(A.8)}$$

When combined, the above two equations yield $v = 1.08a$, which is close to the commonly-employed relation $v = a$. The measured values of the area fraction directly give the volume fraction for use in Eq. (A.1) top give the stoichiometry deviation (x) at each point.

References

[1] M.S. Veshchunov and P. Hofmann, J. Nucl. Mater. 209 (1994) 27.
[2] D.R. Olander, J. Nucl. Mater. 224 (1995) 254.
[3] M.S. Veshchunov, P. Hofmann and A.V. Berdyshev, J. Nucl. Mater. 231 (1996) 1.
[4] K.T. Kim and D.R. Olander, J. Nucl. Mater. 154 (1988) 85.
[5] A.S. Bayoglu and R. Lorenzelli, J. Nucl. Mater. 79 (1979) 437.

[6] Hj. Matzke, J. Chem. Soc. Faraday Trans. II 83 (1987) 1121.
[7] K. Kim and D.R. Olander, J. Nucl. Mater. 102 (1981) 192.
[8] D.R. Olander, J. Nucl. Mater. 110 (1982) 352.
[9] P.J. Hayward and I.M. George, J. Nucl Mater. 208 (1994) 43.
[10] W. Breitung, J. Nucl. Mater. 74 (1978) 10.
[11] A.S. Bayoglu and R. Lorenzelli, Solid State Ionics 12 (1984) 53.
[12] D.R. Olander, J. Electrochem. Soc. 131 (1984) 2161.
[13] G.H. Winslow, High Temp. Sci. 5 (1973) 176.
[14] D.R. Olander, Fundamental Aspects of Nuclear Reactor Fuel Elements (National Tech. Info. Service, 1976) p. 432.